Journal of Magnetic Resonance 210 (2011) 192–199

Contents lists available at ScienceDirect

Journal of Magnetic Resonance

journal homepage: www.elsevier.com/locate/jmr

Determination of the ^{14}N quadrupole coupling constant of nitroxide spin probes by W-band ELDOR-detected NMR

Marc Florent, Ilia Kaminker, Vijayasarathi Nagarajan, Daniella Goldfarb *

Department of Chemical Physics, Weizmann Institute of Science, Rehovot 76100, Israel

ARTICLE INFO

Article history:
Received 20 October 2010
Revised 17 February 2011
Available online 8 March 2011

Keywords:
Nitroxide spin probes
EPR
ESR
Pulse EPR
High field EPR
^{14}N nuclear quadrupole interaction
Nuclear frequencies

ABSTRACT

Nitroxide spin probe electron paramagnetic resonance (EPR) has proven to be a very successful method to probe local polarity and solvent hydrogen bonding properties at the molecular level. The g_{xx} and the ^{14}N hyperfine A_{zz} principal values are the EPR parameters of the nitroxide spin probe that are sensitive to these properties and are therefore monitored experimentally. Recently, the ^{14}N quadrupole interaction of nitroxides has been shown to be also highly sensitive to polarity and H-bonding (A. Savitsky et al., J. Phys. Chem. B 112 (2008) 9079). High-field electron spin echo envelope modulation (ESEEM) was used successfully to determine the P_{xx} and P_{yy} principal components of the ^{14}N quadrupole tensor. The P_{zz} value was calculated from the traceless character of the quadrupole tensor. We introduce here high-field (W-band, 95 GHz, 3.5 T) electron–electron double resonance (ELDOR)-detected NMR as a method to obtain the ^{14}N P_{zz} value directly, together with A_{zz}. This is complemented by W-band hyperfine sublevel correlation (HYSCORE) measurements carried out along the g_{xx} direction to determine the principal P_{xx} and P_{yy} components. Through measurements of TEMPOL dissolved in solvents of different polarities, we show that A_{zz} increases, while $|P_{zz}|$ decreases with polarity, as predicted by Savitsky et al.

1. Introduction

Nitroxide spin labels are well established as excellent sensors of their environment in various systems ranging from material surfaces and pores, soft matter and supramolecular chemistry to a variety of biological systems [1,2]. They have been extensively used to probe molecular motions providing information on local viscosity and ordering mainly through line shape analysis [3,4]. In addition, the sensitivity of the ^{14}N hyperfine coupling (A_{zz} or a_{iso}) to the polarity of the probe environment has been successfully used to determine polarity profiles of membranes [5,6], to monitor water penetration depth in a variety of heterogeneous systems such as membranes and micelles [7–11], and to understand the conformation of proteins [12]. The possibility to resolve the g_{xx} component of the g-tensor by high field EPR has also allowed separating the polarity and proticity of the local environment [13,14]. While it is known that in apolar solvents A_{zz} is very sensitive to the dielectric constant ε, in polar solvent ($\varepsilon > 25$) A_{zz} is mostly dependent on the proticity (H-bonding capability), there is no efficient method to differentiate between polarity and proticity just by the hyperfine interaction [15]. The A_{zz} value can be easily determined from the EPR spectrum, recorded both at conventional magnetic fields (X-band, 9.5 GHz, ~0.35 T) and at higher fields. In contrast, resolving the g_{xx} and g_{yy} values require high field measurements [15,16].

Recently, Savitsky et al. [17] showed that yet another magnetic interaction, the ^{14}N quadrupole interaction (nqi), described by the nuclear quadrupole tensor, **P**, can be used to probe the local environment of nitroxides. Here, hydrogen bonds are expected to have a significant effect on the quadrupole coupling constant e^2qQ/h and the asymmetry parameter η $((P_{xx} - P_{yy})/P_{zz})$. Consequently, this interaction can be used to differentiate between polarity and proticity. The method they used to determine the nqi was electron-spin echo envelope modulation (ESEEM) carried out at W-band (95 GHz, ~3.5 T). At this magnetic field, the A_{xx} and A_{yy} values of nitroxides are around 13–20 MHz and comparable to the ^{14}N Larmor frequency, $\nu_I \sim 10$ MHz. This yields intense enough nuclear modulations that can provide the ^{14}N frequencies along the x and y principal axes of **A**, which to a good approximation coincide with those of **g** [18]. These nuclear frequencies, in turn provide the nqi splitting along these directions. Savitsky et al. [17] carried out ESEEM measurements at different magnetic fields in the g_{xx} and g_{yy} region and obtained P_{xx} and P_{yy}. No information could be obtained at the g_{zz} region because of the large value of A_{zz} (~100 MHz) which prevents the observation of nuclear modulations. The value of P_{zz} was calculated from the traceless nature of the quadrupole tensor under the assumption that the principal axes of **P** and **g** coincide. These authors also carried out quantum chemical calculations to explore the effect of hydrogen bonding

* Corresponding author. Fax: +972 8 9344123.
E-mail address: daniella.goldfarb@weizmann.ac.il (D. Goldfarb).

1090-7807/$ - see front matter © 2011 Elsevier Inc. All rights reserved.
doi:10.1016/j.jmr.2011.03.005

to the NO group on e^2qQ/h and η. The calculations have confirmed that the principal axis system of **g**, **A** and **P** coincides (up to a 15° out of plane position of the NO). The additional electric field induced by the H-bond along the x direction ($2p_x^N$ is the orbital involved in the strong NO σ-bond) results in a strong decrease of $|P_{yy}|$ and $|P_{zz}|$, whereas P_{xx} is only weakly affected. This also leads to an increase in the asymmetry parameter η. The existence of such H-bonds has been observed experimentally through ^{2}H ESEEM, and ^{2}H high field ENDOR (electron-nuclear double resonance) [19].

Savitsky et al. [17] reported that qualitatively, P_{yy} has the same probing properties as A_{zz} in detecting polarity and proticity effects, and showed that it is relatively insensitive to structural and temperature variations. Moreover it is exclusively dependent on the electronic charge distribution of the NO bond and, therefore, it is particularly qualified for polarity studies in nonbonding as well as H-bonding situations. Their calculations showed that P_{yy} is the most sensitive to changes in polarity in terms of a relative change; however the absolute change in terms of frequency shifts is comparable to that of P_{zz}. Therefore, in terms of experimental practicalities it may be easier to determine P_{zz}, depending on the experiment of choice. In this work we show that using ELDOR (electron–electron double resonance)-detected NMR at W-band A_{zz} and P_{zz} can be readily determined.

ELDOR-detected NMR is yet another method to measure nuclear frequencies [20]. Other common methods are ENDOR (electron-nuclear double resonance) and ESEEM. It has been proposed 15 years ago and first demonstrated at X-band frequencies. However, because of the relatively low nuclear Larmor frequencies at ~0.35 T, this method has not been very popular, unless large hyperfine couplings were involved. At higher fields, such as those encountered at Q- and W-band the experiment is more effective due to the increased nuclear Larmor frequencies, especially for low γ nuclei [21–23]. One of the earliest applications of ELDOR-detected NMR has been to nitroxides, where a correlation between the nitrogen ^{15}N nuclear frequencies and the magnetic field have been obtained, yielding the angle between the **g** and **A** tensors, found to be 4° [23].

The ELDOR-detected NMR pulse sequence is shown in Fig. 1. The high turning angle (HTA) pulse, with frequency ν_1, transfers populations across a forbidden EPR transition (ΔM_S=1, ΔM_I = 1, 2, ...). This reduces the population difference across the corresponding allowed transition (ΔM_S = 1, ΔM_I = 0) that is detected either via a free induction decay (FID) produced with a long selective pulse or with a two-pulse echo detection sequence with frequency of ν_2. The spectrum is acquired by measuring the FID or echo intensity as a function of $\Delta\nu = \nu_1 - \nu_2$. In practice ν_1 is swept, while ν_2 is kept constant. Details on the optimization of the S/N and resolution of the experiment can be found in Ref. [24]. In contrast to W-band ESEEM used to determine P_{xx} and P_{yy}, which requires short $\pi/2$ microwave pulses that are difficult to achieve with the available mw power on commercial W-band spectrometers, the power requirements for the ELDOR-detected NMR are very mild.

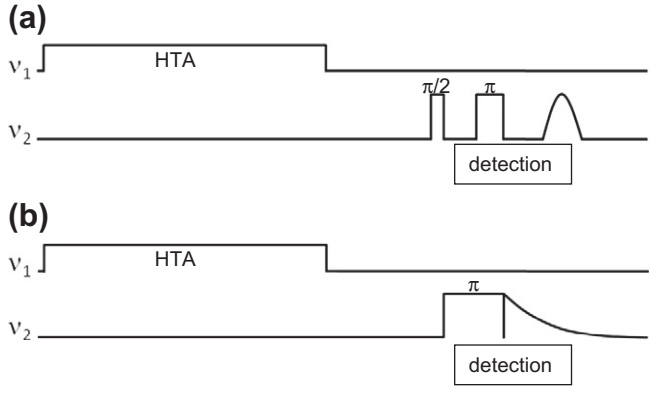

Fig. 1. The ELDOR-detected NMR pulse sequences with (a) echo detection and (b) FID detection.

In the following we describe the energy level diagram of a S = 1/2, I = I system, that is relevant for the nitroxide case and describe the expected appearance of the ELDOR-detected NMR spectra under various conditions.

1.1. The energy level diagram for S = 1/2, I = 1

Fig. 2a shows the energy levels diagram for a S = 1/2, I = 1 spin system for the strong coupling case, $A > 2\nu_I$, where A is the hyperfine splitting. The six energy levels are marked with $|\beta,+1\rangle$, $|\beta,0\rangle$, $|\beta,-1\rangle$ for the lower electron spin manifold and $|\alpha,+1\rangle$, $|\alpha,0\rangle$, $|\alpha,-1\rangle$ for the upper one. The three green solid arrows correspond to the three allowed EPR transitions for $M_I = -1, 0, +1$. The forbidden transitions are marked by dotted lines. Each allowed transition is associated with four forbidden transitions and the frequency difference between the allowed and forbidden transitions give the nuclear frequencies, marked by solid red arrows. These are summarized in Table 1.

The first order expressions for the ^{14}N nuclear frequencies for $A > 2\nu_I$, are:

$$\nu^{\alpha}_{sq1} = A/2 - \nu_I - 3P/2 \quad (1a)$$
$$\nu^{\alpha}_{sq2} = A/2 - \nu_I + 3P/2 \quad (1b)$$
$$\nu^{\alpha}_{dq} = A - 2\nu_I \quad (1c)$$
$$\nu^{\beta}_{sq1} = A/2 + \nu_I - 3P/2 \quad (1d)$$
$$\nu^{\beta}_{sq2} = A/2 + \nu_I + 3P/2 \quad (1e)$$
$$\nu^{\beta}_{dq} = A + 2\nu_I \quad (1f)$$

where A and P are the orientation dependent hyperfine and nuclear quadrupole couplings, and $P_{zz} = e^2qQ/[2hI(2I-1)]$. The value of P can be determined from any of the following relationship:

$$\nu^{\alpha}_{dq} - 2\nu^{\alpha}_{sq1} = 3P \quad (2a)$$
$$\nu^{\alpha}_{dq} - 2\nu^{\alpha}_{sq2} = -3P \quad (2b)$$
$$\nu^{\beta}_{dq} - 2\nu^{\beta}_{sq1} = 3P \quad (2c)$$
$$\nu^{\beta}_{dq} - 2\nu^{\beta}_{sq2} = -3P \quad (2d)$$

$$\nu^{\alpha}_{sq2} - \nu^{\alpha}_{sq1} = 3P \quad (3a)$$
$$\nu^{\beta}_{sq2} - \nu^{\beta}_{sq1} = 3P \quad (3b)$$

$$\nu^{\beta}_{sq1} - \nu^{\alpha}_{sq2} = 2\nu_I - 3P \quad (4a)$$
$$\nu^{\beta}_{sq2} - \nu^{\alpha}_{sq1} = 2\nu_I + 3P \quad (4b)$$

The hyperfine coupling can be obtained from

$$\nu^{\beta}_{sq1} + \nu^{\alpha}_{sq2} = A \quad (5a)$$
$$\nu^{\beta}_{sq2} + \nu^{\alpha}_{sq1} = A \quad (5b)$$

When the magnetic field is set to canonical x, y, or z directions the corresponding principal components of **A** and **P** can be obtained. The first order expressions are usually valid when $|\nu_I \pm A| \gg P$. This applies for the z direction for both manifolds and only for the β manifold for the x, y directions. As long as the experiment is selective with respect to the ^{14}N hyperfine component (see Table 1), as usually possible for the z direction where A_{zz} is large, negative and positive frequencies in the ELDOR-detected NMR spectrum are distinguishable.

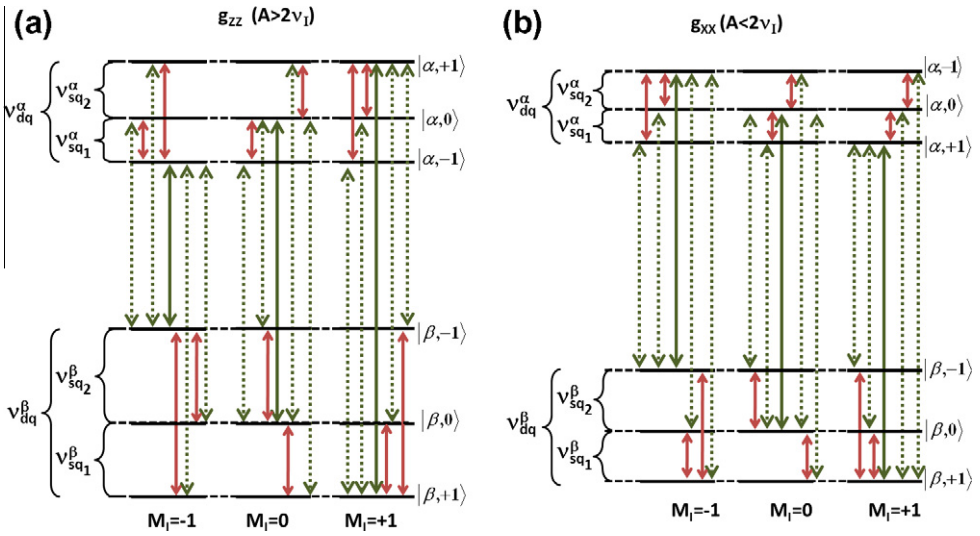

Fig. 2. Energy levels diagram of a nitroxide with $P > 0$, $A > 0$ and (a) $A > 2\nu_I$, as it is the case along the g_{zz} direction, or (b) $A < 2\nu_I$, as it is the case along the g_{xx} direction.

Table 1
Summary of the allowed transitions and the associated forbidden transitions, the nuclear frequencies generated by their differences and the side of the ELDOR-detected NMR spectrum they appear at ($\Delta\nu$ positive or negative), for $A > 2\nu_I$ (Fig. 2a).

Allowed EPR transition, M_I	Forbidden transition $\Delta M_I = \pm1$	Forbidden transition $\Delta M_I = \pm2$	Nuclear frequency $\Delta\nu > 0$	Nuclear frequency $\Delta\nu < 0$
−1	$\|\beta,-1\rangle \rightarrow \|\alpha,0\rangle$	$\|\beta,-1\rangle \rightarrow \|\alpha,+1\rangle$	ν^{α}_{sq1}, ν^{α}_{dq}	
	$\|\alpha,-1\rangle \rightarrow \|\beta,0\rangle$	$\|\alpha,-1\rangle \rightarrow \|\beta,+1\rangle$	ν^{β}_{sq2}, ν^{β}_{dq}	
0	$\|\beta,0\rangle \rightarrow \|\alpha,+1\rangle$		ν^{α}_{sq2}	ν^{α}_{sq1}
	$\|\beta,0\rangle \rightarrow \|\alpha,-1\rangle$		ν^{β}_{sq1}	ν^{β}_{sq2}
	$\|\alpha,0\rangle \rightarrow \|\beta,+1\rangle$			
	$\|\alpha,0\rangle \rightarrow \|\beta,-1\rangle$			
+1	$\|\beta,+1\rangle \rightarrow \|\alpha,0\rangle$	$\|\beta,+1\rangle \rightarrow \|\alpha,-1\rangle$		ν^{α}_{sq2}, ν^{α}_{dq}
	$\|\alpha,+1\rangle \rightarrow \|\beta,0\rangle$	$\|\alpha,+1\rangle \rightarrow \|\beta,-1\rangle$		ν^{β}_{sq1}, ν^{β}_{dq}

2. Materials and methods

2.1. Sample preparation

The spin probes used were 4-hydroxy-2,2,6,6-tetramethylpiperidinyloxy (TEMPOL, purchased from Aldrich Chem Co), and 2,2,5,5-tetramethyl-1-pyrrolidinyloxy-3-carboxylic acid (3CP, purchased from Acros Organics). The solvents used were: toluene, deuterated toluene, doubly deionized water–ethanol 1:1 mixture, 2-propanol and glycerol. Quartz capillaries were filled with 1 mM or 2.5 mM solutions of spin probes and then frozen by immersion in the precooled cryostat at 40 K.

2.2. EPR measurements

All measurements were carried out on a home-built W-band spectrometer operating at 94.9 GHz with a two-channel microwave bridge [25]. Echo detected (ED) EPR spectra were recorded using the two-pulse echo sequence, with $t_{\pi/2}$ and t_π pulses of 100 and 200 ns respectively, and $\tau = 500$ ns. A temperature of 40 K was chosen because it is within the usual range of working temperatures for nitroxides, which give the higher signal-to-noise ratio. It has been shown that lowering the temperature further will just increase T_1 while leaving T_2 almost unaffected [26].

The proton Larmor frequency, determined by Mims ENDOR [27] with $t_{\pi/2}$=15 ns and a radiofrequency (RF) pulse of 15 μs, was used to precisely determine the external magnetic field.

ELDOR-detected NMR spectra were recorded with a HTA pulse of 500 μs, with a B_1 of about 12 MHz at the center of the spectrum ($\Delta\nu = 0$), and ~2 MHz at the edges of the spectrum. A two-pulse echo detection, $t_{\pi/2} = 100$ ns, $t_\pi = 200$ ns and τ of 500 ns, or a FID detection, with a pulse of 1 μs (cf. Fig. 1) were used. "Full" ELDOR-Detected NMR spectra were recorded in the range of $\nu_0 \pm 195$ MHz with $\nu_0 = 94.9$ GHz and with a step, δ, of 0.975 MHz per point. For spectra with a range of $\nu_0 \pm 45$ MHz, the step was 0.3 MHz. For better resolution, "partial" spectra were recorded, for $\Delta\nu = 30$–69 MHz, $\Delta\nu = -67.6 - (-56.2)$ MHz and $\Delta\nu = -45.5 - (-6.5)$ MHz with $\delta = 0.065$ MHz, and for $\Delta\nu = 23.4$–72.8 MHz $\delta = 0.08$ MHz was used.

Parallel acquisition of ELDOR-detected NMR spectra was done using a home-made setup allowing rapid change of the magnetic field from one field position to another [28]. In this experiment several field jumps take place within one repetition time, measuring 10 spectra within one repetition time delay between consecutive sequences. The magnetic field position was incremented in two series of five steps, within one repetition time, with the following sequence of changes in the central field, in mT: −2.08; −1.664; −1.248; −0.832; −0.416; −1.872; −1.456; −1.04; −0.624; −0.208. Here the highest magnetic field value was set to the high field edge of the spectrum where the echo is no longer detectable. Each step lasts 2 ms and has a settle time of 1.3 ms prior to signal detection.

HYSCORE (hyperfine sublevel correlation) spectra [29] were recorded using $t_{\pi/2}$ and t_π pulse of 12.5 and 25 ns respectively, and $\tau = 150$ ns. t_1 and t_2 were incremented by 12.5 ns from an initial value of 50 ns. Two dimensional (2D) Fourier transform (magnitude mode) was applied after removal of the decay using a second order polynomial fit, followed by sine-bell window apodization and zero filling to 512 points.

Simulations of the ED-EPR spectra were carried out with the "Pepper" function of the Easyspin toolbox [30] that simulates solid-state CW-EPR spectra. ELDOR-detected NMR spectra were simulated using functions of Easyspin. The spin system used was the same as the one used for simulating the ED-EPR spectra, with just the addition of a quadrupole tensor. All the transitions (allowed and forbidden) were calculated for different field orientations the range of which was determined by the field position within the

EPR spectrum and taking into account a non-zero linewidth due to g-strain. The final spectrum was obtained after taking the difference between the allowed and associated forbidden transitions and summing over all selected orientations. HYSCORE spectra were simulated using Simbud software [31]. All presented simulations were done assuming that the principal axes of **g**, **A** and **P** coincide, with interchanging P_{xx} and P_{yy}.

3. Results and discussion

The W-band ED-EPR spectrum of TEMPOL in toluene (2.5 mM), recorded at 40 K, is shown in Fig. 3. The hyperfine splitting is well resolved in the g_{zz} region, whereas along the g_{xx} and g_{yy} regions the hyperfine splitting is hidden within the inhomogeneous linewidth. The well resolved hyperfine splitting along g_{zz} allowed us to easily select a specific EPR transition. The highest field transition ($M_I = -1$ transition, see Fig. 2) is particularly interesting as its g_{zz} singularity does not overlap with any other transition, as shown by the simulated spectrum, decomposed to its M_I sub-spectra of the allowed EPR transitions in Fig. 3. The following parameters: $g = [2.00988\ 2.00614\ 2.00194]$, and $A = [20.5 \pm 1\ \ 21.75 \pm 1\ \ 98 \pm 1]$ MHz were used in the simulation. The error was estimated from the range of the parameters that could fit the spectra.

The ELDOR-detected NMR spectrum recorded at the $M_I = -1$ component of the g_{zz} singularity is depicted in Fig. 4a. As expected the peaks appear in the $\Delta\nu > 0$ side with $\nu^{\beta}_{sq2} \approx 56.1$ MHz and $\nu^{\alpha}_{sq1} \approx 40.5$ MHz. The assignment is based on the knowledge of the positive sign of A from the literature [32]. The weak peaks at 75.3 and 117.8 MHz are assigned to ν^{α}_{dq}, and ν^{β}_{dq}, respectively. From these frequencies, and using Eqs. (2a), (2d), (4b), we obtained $P_{zz} = -1.9, -1.8, -1.75$ MHz, respectively. The sign of P_{zz} arises directly from the calculation. Here ν_I was determined from the ^{1}H Larmor frequency measured using Mims ENDOR at the same field position. An unexpected peak appears around 96 MHz and it most probably arises from another allowed EPR transitions ($M_I = 0$) that is also affected by the HTA pulse through cross relaxation, which can occur during the long HTA pulse. Indeed, the EPR transitions are separated by A, which is 98 MHz.

The uncertainty in the line positions in the ELDOR-detected NMR spectrum increases as the linewidth increases. This in turn, increases the error in 3P, which is the difference between the frequencies of two broad lines. The linewidth can be narrowed, at the expense of signal-to-noise ratio (S/N) by detecting via FID rather than by echo detection. Using echo detection with longer pulse length also decreases the linewidth, with a much less dramatic effect on the S/N ratio (see Fig. S1 in supplementary information) and these are the experimental conditions we chose.

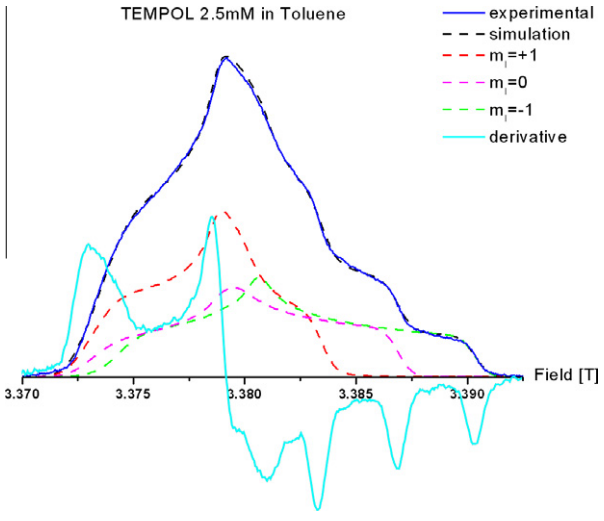

Fig. 3. ED-EPR spectrum of TEMPOL in toluene recorded at W-band, with its derivative and simulation. The decomposition into the three M_I dependent transitions are shown as well. The simulation parameters are given in the text.

Because of the large hyperfine anisotropy the choice of the magnetic field setting for the measurement is an important feature, especially when the reproducibility required for comparison of different spectra is concerned. This is demonstrated in Fig. 5a, where the ELDOR-detected NMR spectrum in the range of 25–65 MHz is depicted as a function of the field within a small field range of about 20 G around the g_{zz} position of the $M_I = -1$ transition. Significant shifts of the peaks' positions are clear, showing that the selection of the observing field position is of prime importance. The 2D plot was recorded using the parallel acquisition mode. The corresponding stack plot is depicted in Supplementary information, Fig. S2. From the positions of these peaks we have calculated the field dependence of A and P as shown in Fig. 6. A_{zz} increases with the field as expected, yielding a maximum value of 97 MHz which is assigned to A_{zz}. The A_{zz} value obtained from the ED-EPR spectrum is 98 MHz and is in good agreement with this value. The field dependence of $|P|$ is shown in Fig. 6 as well. The largest value obtained for $|P|$ should yield P_{zz}. Here the relative error is larger because P is determined by differences between two large quantities. Starting from low magnetic field, $|P|$ decreases with the field, probably due to some overlap with other transitions, then $|P|$ go through a plateau, before decreasing again at high field, which could be an effect of an increase in the error due to the very low S/N ratio at the spectrum edge. In the part where P does not change much, its value is -1.77 ± 0.1 and therefore we take the plateau value as P_{zz} and determined $e^2qQ/h = -3.54 \pm 0.2$ MHz. In principle, the observed decrease of P with the field could indicate the g and quadrupole tensors are not collinear. The DFT calculations carried out by Savitsky et al. [17] for a proxyl nitroxide showed that g, A and P are colinear. We do not expect a very different result for TEMPOL nitroxide, and indeed only a deviation of at most 4° has been reported for a TEMPOL radical in polymer matrix, between g_{zz} and A_{zz} [23]. Moreover, we tried to reproduce the observed trend using simulations with non-colinear tensors but we could not reproduce this strong dependence. For up to an angle of 25° between P_{zz} and g_{zz} a variation of no more than 0.2 MHz in 3P was observed within the field range shown in Fig. 6.

A simulation of the ELDOR-detected NMR spectrum as a function of the field is shown in Fig. 5b. This simulation was done using the P_{zz} value found experimentally (see above), $P_{xx} = 0.48$ $P_{yy} = 1.29$ MHz, and the EPR parameters used to simulate the ED-EPR spectrum. The P_{xx} and P_{yy} values were determined from HYSCORE spectra (see below). The simulations did not take into account the experimental conditions, namely the length of the HTA and its B_1 which strongly affects the relative intensities in the ELDOR-detected NMR spectrum; therefore we focused only on the peak frequencies. We can see that at low fields, close to the $M_I = 0$ transition, the peaks broaden and the frequencies change with the field. This is a consequence of the large anisotropy and overlap with the $M_I = 0$ sub-spectrum. At higher fields, we can see that the frequencies are still shifting with the field, though not as much as in the experiment. The simulation shows that the peaks are not symmetrical, which adds to the uncertainty of the peak position, especially when there are some baseline problems. Furthermore, this asymmetry increases when going to lower field, therefore increasing the error in the frequencies of the peaks at lower field.

Fig. 4b shows the ELDOR-detected NMR spectrum measured at the g_{zz} singularity of the $M_I = 0$ component. Here according to Table 1, all the single quantum transitions are observed; two in the $\Delta\nu < 0$ side, and two in the $\Delta\nu > 0$ side. Now P can be calculated

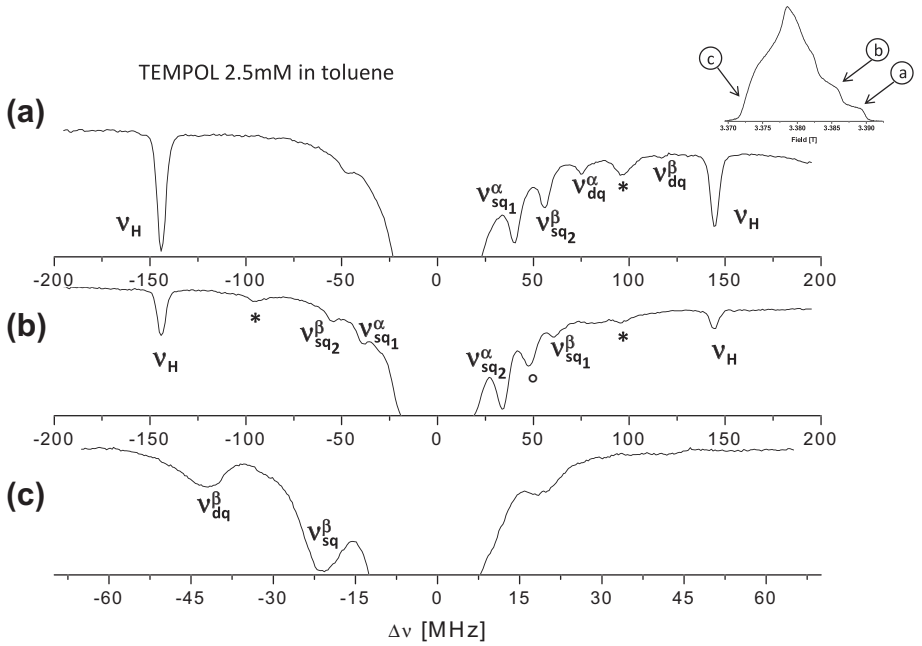

Fig. 4. ELDOR-detected NMR spectra of TEMPOL in toluene recorded at (a) the $M_I = -1$ transition and (b) the $M_I = 0$ transition, along the g_{zz} direction, and (c) along the g_{xx} direction, where the hyperfine splitting cannot be resolved. Inset: Echo detected EPR spectrum with the three positions where ELDOR-detected NMR spectra where recorded.

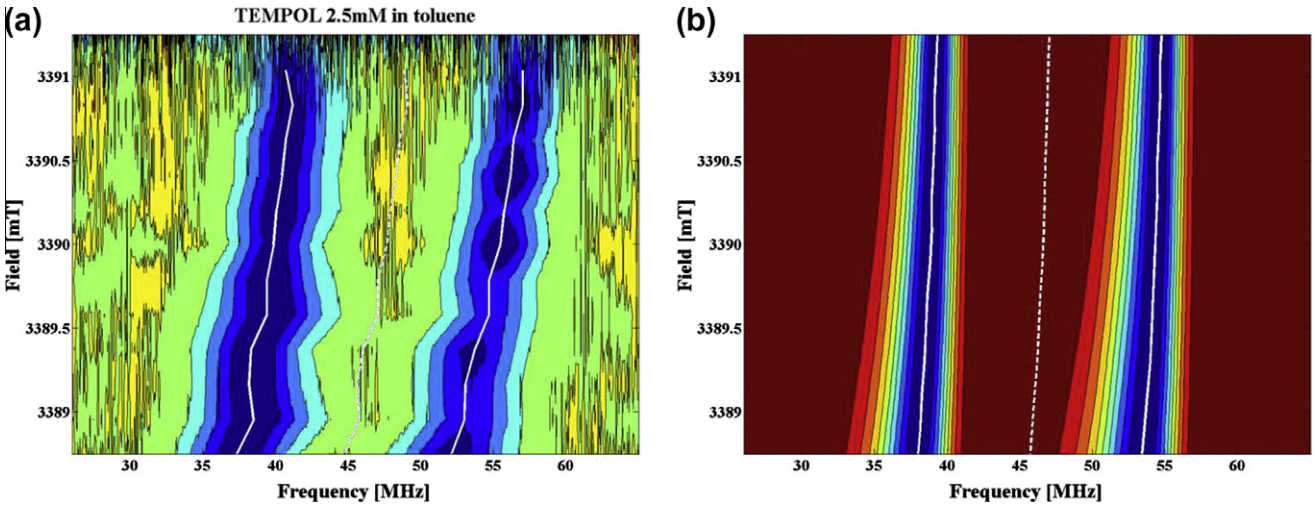

Fig. 5. (a) Two dimensional ELDOR-detected NMR spectrum of TEMPOL in toluene recorded around the $M_I = -1$ component of the g_{zz} singularity. (b) Simulation using the EPR parameters found in the ED-EPR simulation and fitting **P** (see text).

using Eqs. (3) and (4). At this field, marked with (b) in the inset of Fig. 4, there are also contributions from the $M_I = -1$ component for orientations of $\theta > 0°$. These peaks appear in the $\Delta\nu > 0$ side (they are marked with °). They are shifted with respect to those observed in the spectrum shown in Fig. 4a due to the change in field and selection of orientations slightly away from the z axis for $M_I = -1$. The ν^{β}_{sq1}, ν^{β}_{sq2}, ν^{α}_{sq1} and ν^{α}_{sq2} frequencies obtained from the $M_I = 0$ spectrum appear at 61.1 MHz, −54.21 MHZ, −37.7 MHz and 33.67 MHz, respectively. Using Eqs. (3) and (4) we confirm that P_{zz} is negative. The value of P_{zz}, however, was found to strongly depend on the frequencies used in Eqs. (3) or (4). Eq. (3) yields $P_{zz} = -2.3$ and $P_{zz} = -1.3$, depending upon considering ν^{β}_{sq1} and ν^{β}_{sq2} (Eq. (3b)), or ν^{α}_{sq1} and ν^{α}_{sq2} (Eq. (3a)), respectively. Similarly, Eq. (4) yields $P_{zz} = -2.2$ and $P_{zz} = -1.4$, depending upon considering ν^{α}_{sq1} and ν^{β}_{sq2} (Eq. (4b)), or ν^{α}_{sq2} and ν^{β}_{sq1} (Eq. (4a)), respectively. This is a rather broad range of P values and the discrepancy may be attributed to the overlap of $M = -1$, that give parasitic peaks on the positive side of the spectrum. Similarly to P, the A values determined in the case of $M_I = 0$ selection are in the range of 91.91–94.77 MHz. We attribute this to some measurement uncertainty due to the resolution and contribution from the $M_I = -1$ transition, but farther from its z component.

The conclusion from this section is that A_{zz} and P_{zz} are best obtained by setting the magnetic field to the $M_I = -1$ g_{zz} singularity, as determined by the derivative EPR spectrum (see Fig. 3) and using Eq. (2), whenever the double quantum transition can be detected. In terms of frequency, the maximum of the $M_I = -1$ g_{zz} singularity of the derivative EPR spectrum, corresponds to the middle of the 2D ELDOR-detected NMR spectrum. When Eq. (4) is used, the error is larger because it involves also the error in determining ν_I.

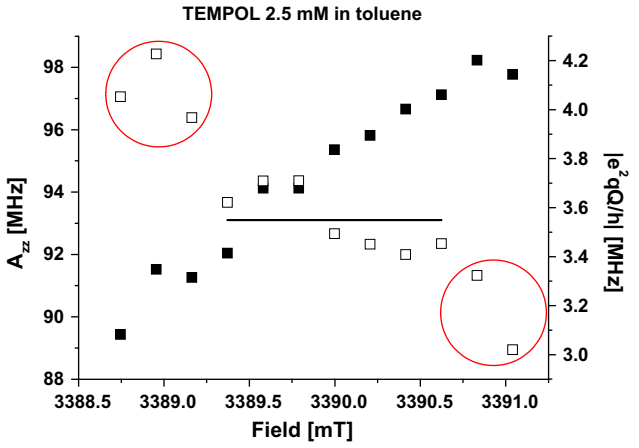

Fig. 6. The field dependence of A (■) and P (□) measured by ELDOR-detected NMR along the g_{zz} direction of the $M_I = -1$ component.

In order to determine P_{xx}, a spectrum was recorded at the lowest possible field near g_{xx}. At this region the individual M_I transitions are not resolved due to the small A_{xx} value. However, if the field is set to the outmost field edge some selection may still be possible. The ELDOR-detected NMR spectrum, depicted in Fig. 4c, shows as expected, that the transitions appear at lower frequencies compared to the spectrum recorded at the g_{zz} region, and actually most of them are lost in the broad $\Delta\nu = 0$ peak. Yet, we can still distinguish two broad peaks assigned to ν^{β}_{dq} and ν^{β}_{sq1} at −41.9 MHz and −20.7 MHz, respectively. Another peak appears on the positive side of the spectrum around 19 MHz, which is probably ν^{β}_{sq1} or ν^{β}_{sq2}. The presence of this peak on the positive side shows that the different components of the transition cannot be separated at this region of the spectrum.

The HYSCORE experiment may be a good alternative to ELDOR-detected NMR for determining P_{xx}. It is also richer in terms of information content with respect to one dimensional ESEEM. The cross peaks in the two dimensional HYSCORE spectrum reveal correlations between nuclear frequencies belonging to different electron spin manifolds, namely the α and β manifolds. Fig. 7 shows the HYSCORE spectrum of TEMPOL in toluene recorded at the g_{xx} position and its simulation. The spectrum shows curved cross peaks due to the contributions of a range of field orientations and the large anisotropy of **A**. These are assigned on Fig. 7, and we can see for example a long ridge for $(\nu^{\alpha}_{sq2}, \nu^{\beta}_{sq1})$ instead of a single peak. The peaks on the (+, +) diagonal at 17.97 MHz and 21.85 MHz give ν^{β}_{sq1} and ν^{β}_{sq2} and are in good agreement with the 19 and 20.7 MHz values obtained from the ELDOR-detected NMR spectrum. From this values we can estimate $P_{xx} = 1.3$ MHz. The simulation, shown in Fig. 7b, was done using, as previously, $g = [2.00988\ 2.00614\ 2.00194]$, $A = [20.5\ 21.75\ 98]$ MHz, and $e^2qQ/h = -3.54$ MHz and $\eta = 0.46$. In the simulation we could reproduce the peaks' frequencies, but not their relative intensities. For example the peak around (22, 4.8) MHz which appears in the (−, +) quadrant in the experimental spectrum, appears in the positive quadrant in the simulation (and is hardly present in the negative quadrant). But they correspond to the same correlated coherence.

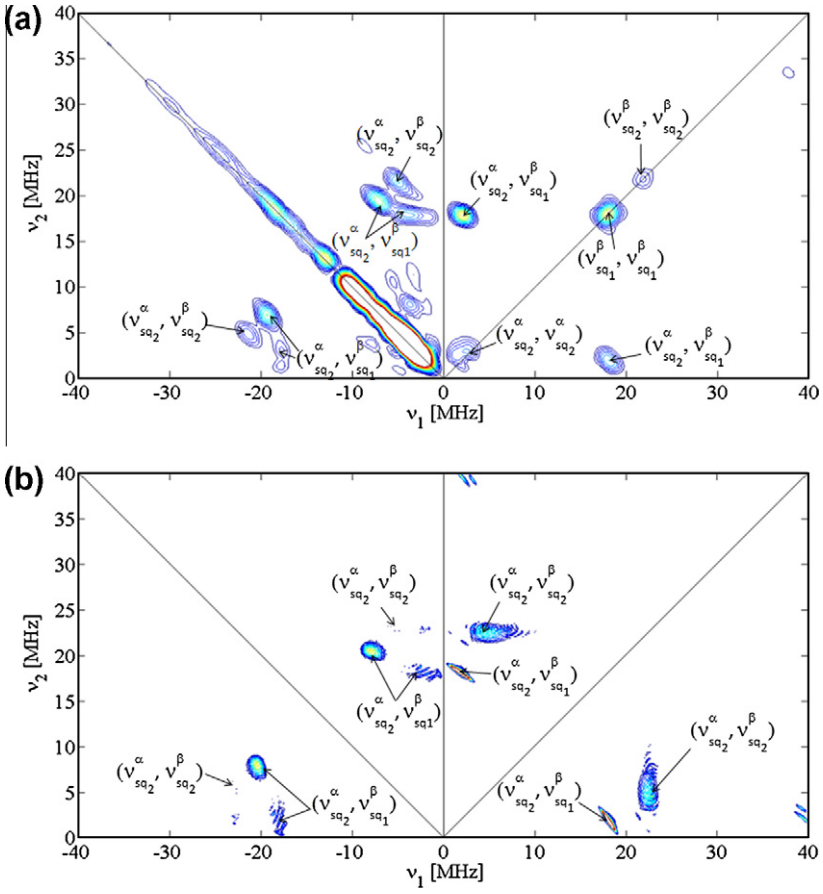

Fig. 7. (a) W-band HYSCORE spectrum of TEMPOL in toluene recorded along the g_{xx} direction, (3372.5 mT) and (b) its simulation. The parameters used in the simulations are given in the text.

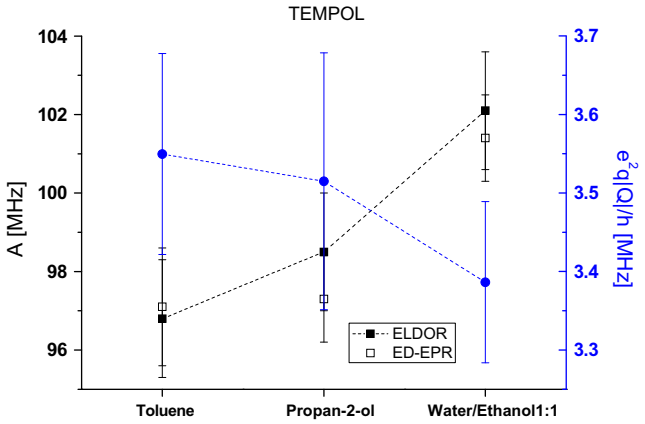

Fig. 8. A_{zz} values of TEMPOL in three different solvents determined from the echo detected EPR spectrum (□) and by ELDOR-detected NMR (■), and P measured by ELDOR-detected NMR (●), along the g_{zz} direction of the $M_I = -1$ transition.

Finally, measurements were carried out in two other solvents to see whether the accuracy of the measurements is sufficient to resolve the effect of polarity and of hydrogen bonding on the value of P_{zz}. The results are reported in Fig. 8. The A_{zz} value increases with the polarity of the solvent as expected, while $|P_{zz}|$ decreases as predicted by Savitsky et al. [17] The uncertainty in P_{zz} is however rather large and close to the differences between the samples.

We have also carried out measurements of 3CP in glycerol and compared our results with those of Savitsky et al. [17]. The spin label is somewhat different, as we have a carboxylic acid function where they have used an alcohol, but we do not expect difference in the coupling constant. The values we obtained are (P_{xx}, P_{yy}, P_{zz}) = (0.11 ± 0.9, 1.56 ± 0.6, −1.67 ± 0.3) MHz compared to (0.36, 1.23, −1.59) MHz reported by Savitsky et al. [17], with P_{yy} being along g_{xx}. There is a good agreement for P_{zz} but less for P_{xx} and P_{yy}. The very large error in the P_{xx} and P_{yy} values stems from the ELDOR-detected NMR method used to determine these values. It is not appropriate for the g_{xx} direction as showed above. The A_{zz} value measured is 101.7 MHz with our method, quite similar to their 101.40 MHz.

The smaller error reported by Savitsky et al. arises from the use of a perdeuterated nitroxide, where the T_2 is very long. Such a probe could also improve the ELDOR-detected NMR resolution that is T_2 dependent but this is not practical in terms of cost for widespread applications.

4. Conclusions

We have shown that high field ELDOR-detected NMR can be used to measure the P_{zz} component of the ^{14}N nuclear quadrupole tensor of nitroxide spin labels and the quadrupole coupling constant that is directly derived from it. The application of the method to TEMPOL in solvents of different polarities show the P_{zz} can be determined with accuracy just sufficient to resolve the polarity effect due to resolution limitations. The determination of the asymmetry parameter requires the determination of either P_{xx} or P_{yy} and for those ELDOR-detected NMR does not perform well due to resolution limitations and these should be determined from W-band ESEEM or HYSCORE complementary measurements. W-band ENDOR is not as appropriate for this because of the difficulties to determine very low frequencies.

The ELDOR-detected NMR experiment has the advantage that its mw power requirements are rather low, as compared to the ESEEM and HYSCORE experiments applied to nitroxides, where short enough pulses, that cover both allowed and forbidden transitions are essential. So far commercial W-band spectrometers have been limited in power and ESEEM or HYSCORE measurements may not be feasible while ELDOR-detected NMR is if a second microwave channel is available. In principle W-band ENDOR can provide P_{zz} as well, but the hardware requirements are more demanding than those of ELDOR-detected NMR in terms of probe head design and the RF components needed, particularly an RF amplifier. Some pulse spectrometers lack ENDOR capabilities. In addition, the sensitivity is expected to be lower, though the resolution higher. Moreover, the observation of the double quantum nuclear transitions is very difficult in ENDOR. In ELDOR-detected NMR there is some resolution improvement due to the spread of the signals in the positive and negative sides which is meaningful when the HTA pulse is selective with respect to the M_I values. Some further resolution improvement may be expected by using deuterated solvents thereby lengthening the electron spin phase memory time, which determines the resolution of the ELDOR-detected NMR spectrum.

Measurements of P_{zz} by ELDOR-detected NMR at X-band will be limited by the small ^{14}N Larmor frequency (∼1 MHz) which will reduce the resolution considerably. We expect the method to work well at Q-band and up, where the Larmor frequency is large enough and the A_{zz} features of the $M_I = -1$ is well resolved.

Appendix A. Supplementary material

Supplementary data associated with this article can be found, in the online version, at doi:10.1016/j.jmr.2011.03.005.

References

[1] S. Schlick, Advanced ESR Methods in Polymer Research, Wiley, 2006.
[2] M. Brustolon, E. Giamello, Electron Paramagnetic Resonance: A Practitioners Toolkit, Wiley, 2009.
[3] D.J. Schneider, J.H. Freed, Spin Labeling: Theory and Applications, Plenum, New-York, 1989.
[4] J.D. Morisett, Spin Labeling: Theory and Applications, Academic Press, New-York, 1976.
[5] D. Kurad, G. Jeschke, D. Marsh, Lipid membrane polarity profiles by high-field EPR, Biophys. J. 85 (2003) 1025–1033.
[6] D. Marsh, Polarity and permeation profiles in lipid membranes, Proc. Natl. Acad. Sci. USA 98 (2001) 7777–7782.
[7] O.H. Griffith, P.J. Dehlinger, S.P. Van, Shape of hydrophobic barrier of phospholipid bilayers (evidence for water penetration in biological-membranes), J. Membrane Biol. 15 (1974) 159–192.
[8] A. Caragheorgheopol, H. Caldararu, I. Dragutan, H. Joela, W. Brown, Micellization and micellar structure of a poly(ethyleneoxide)/poly(propyleneoxide)/poly(ethyleneoxide) triblock copolymer in water solution, as studied by the spin probe technique, Langmuir 13 (1997) 6912–6921.
[9] S. Ruthstein, V. Frydman, D. Goldfarb, Study of the initial formation stages of the mesoporous material SBA-15 using spin-labeled block co-polymer templates, J. Phys. Chem. B 108 (2004) 9016–9022.
[10] D. Marsh, Membrane water-penetration profiles from spin labels, Eur. Biophys. J. Biophys. Lett. 31 (2002) 559–562.
[11] A.M. Wasserman, Spin probes in micelles, Usp. Khim. 63 (1994) 391–401.
[12] W.L. Hubbell, D.S. Cafiso, C. Altenbach, Identifying conformational changes with site-directed spin labeling, Nat. Struct. Biol. 7 (2000) 735–739.
[13] H.J. Steinhoff, A. Savitsky, C. Wegener, M. Pfeiffer, M. Plato, K. Möbius, High-field EPR studies of the structure and conformational changes of site-directed spin labeled bacteriorhodopsin, BBA-Bioenergetics 1457 (2000) 253–262.
[14] D. Marsh, Spin-label epr for determining polarity and proticity in biomolecular assemblies: transmembrane profiles, Appl. Magn. Reson. 37 (2010) 435–454.
[15] R. Owenius, M. Engström, M. Lindgren, M. Huber, Influence of solvent polarity and hydrogen bonding on the EPR parameters of a nitroxide spin label studied by 9-GHz and 95-GHz EPR spectroscopy and DFT calculations, J. Phys. Chem. A 105 (2001) 10967–10977.
[16] E. Bordignon, H. Brutlach, L. Urban, K. Hideg, A. Savitsky, A. Schnegg, P. Gast, M. Engelhard, E.J.J. Groenen, K. Möbius, H.J. Steinhoff, Heterogeneity in the nitroxide micro-environment: polarity and proticity effects in spin-labeled proteins studied by multi-frequency EPR, Appl. Magn. Reson. 37 (2010) 391–403.
[17] A. Savitsky, A.A. Dubinskii, M. Plato, Y.A. Grishin, H. Zimmermann, K. Möbius, High-field EPR and ESEEM investigation of the nitrogen quadrupole interaction of nitroxide spin labels in disordered solids: toward differentiation between

polarity and proticity matrix effects on protein function, J. Phys. Chem. B 112 (2008) 9079–9090.
[18] M.A. Hemminga, L.J. Berliner, T.I. Smirnova, A.I. Smirnov, High-Field ESR Spectroscopy in Membrane and Protein Biophysics, ESR Spectroscopy in Membrane Biophysics, Springer, US, 2007. pp. 165–251.
[19] T.I. Smirnova, A.I. Smirnov, S.V. Paschenko, O.G. Poluektov, Geometry of hydrogen bonds formed by lipid bilayer nitroxide probes: a high-frequency pulsed ENDOR/EPR study, J. Am. Chem. Soc. 129 (2007) 3476.
[20] P. Schosseler, T. Wacker, A. Schweiger, Pulsed ELDOR detected NMR, Chem. Phys. Lett. 224 (1994) 319–324.
[21] L. Kulik, B. Epel, J. Messinger, W. Lubitz, Pulse EPR, Mn-55-ENDOR and ELDOR-detected NMR of the S-2-state of the oxygen evolving complex in Photosystem II, Photosynth. Res. 84 (2005) 347–353.
[22] I. Kaminker, H. Goldberg, R. Neumann, D. Goldfarb, High-field pulsed EPR spectroscopy for the speciation of the reduced [PV2Mo10O40](6-) polyoxometalate catalyst used in electron-transfer oxidations, Chem.-Eur. J. 16 (2010) 10014–10020.
[23] G. Jeschke, H.W. Spiess, NMR-correlated high-field electron paramagnetic resonance spectroscopy, Chem. Phys. Lett. 293 (1998) 9–18.
[24] A. Potapov, B. Epel, D. Goldfarb, A triple resonance hyperfine sublevel correlation experiment for assignment of electron-nuclear double resonance lines, J. Chem. Phys. 128 (2008) (article number: 052320).
[25] D. Goldfarb, Y. Lipkin, A. Potapov, Y. Gorodetsky, B. Epel, A.M. Raitsimring, M. Radoul, I. Kaminker, HYSCORE and DEER with an upgraded 95 GHz pulse EPR spectrometer, J. Magn. Reson. 194 (2008) 8–15.
[26] G. Jeschke, Y. Polyhach, Distance measurements on spin-labelled biomacromolecules by pulsed electron paramagnetic resonance, Phys. Chem. Chem. Phys. 9 (2007) 1895–1910.
[27] W.B. Mims, Envelope modulation in spin-echo experiments, Phys. Rev. B – Solid State 5 (1972) 2409–2419.
[28] I. Kaminker, M. Florent, B. Epel, D. Goldfarb, Simultaneous acquisition of pulse EPR orientation selective spectra, J. Magn. Reson. 208 (2011) 95–102.
[29] P. Höfer, A. Grupp, H. Nebenführ, M. Mehring, Hyperfine sublevel correlation (Hyscore) spectroscopy – a 2d electron-spin-resonance investigation of the squaric acid radical, Chem. Phys. Lett. 132 (1986) 279–282.
[30] S. Stoll, A. Schweiger, EasySpin, a comprehensive software package for spectral simulation and analysis, EPR. J. Magn. Reson. 178 (2006) 42–55.
[31] A. Astashkin, <http://chem.arizona.edu/rss/epr/software.html>.
[32] M. Tabak, A. Alonso, O.R. Nascimento, Single-crystal electron-spin-resonance studies of a nitroxide spin label. 1. Determination of the *G* and *a* tensors, J. Chem. Phys. 79 (1983) 1176–1184.